




Unconventional magnetic order emerging from competing energy scales in the new RRh_3Si_7 intermetallics ($R = Gd-Yb$)

Long Qian ¹, Shiming Lei,² Binod K. Rai,² C.-L. Huang,² Alannah M. Hallas,³ Gregory T. McCandless,⁴ Julia Y. Chan ⁴ and E. Morosan ^{1,2,*}

¹*Department of Chemistry, Rice University, Houston, Texas 77005 USA*

²*Department of Physics and Astronomy, Rice University, Houston, Texas 77005 USA*

³*Department of Physics and Astronomy and Quantum Matter Institute, University of British Columbia, Vancouver, British Columbia V6T 1Z1 Canada*

⁴*Department of Chemistry, University of Texas at Dallas, Richardson, Texas 75080 USA*



(Received 18 February 2021; accepted 30 August 2021; published 30 September 2021)

The competition between Ruderman-Kittel-Kasuya-Yosida (RKKY), crystal electric field (CEF), and Kondo energy scales has recently emerged at the heart of complex magnetism in several Ce- or Yb-based intermetallics. Hard axis magnetic order has been observed in a handful of these compounds, independent of the crystal symmetry, size of the ordered moment, or the relative scale of the Kondo and magnetic ordering temperatures. This raises the question of the role of each energy scale in driving the ground state properties. In focusing on a single class of compounds, the rhombohedral RRh_3Si_7 , we compare the anisotropy and magnetic ground states in members of this series with only RKKY interactions ($R = Gd$), or RKKY and CEF effects ($R = Tb-Tm$), with the behavior of the $R = Yb$ compound, where all three energy scales (RKKY, CEF, Kondo) are at play. Moreover, we extend the comparison to two other isostructural Kondo systems $YbIr_3Si_7$ and $YbIr_3Ge_7$, where hard axis magnetic order is also observed. The non-Kondo compounds RRh_3Si_7 ($R = Tb-Tm$) lack the complexity of magnetic order along the hard CEF axis, pointing to the dominant role of the Kondo effect in driving this magnetic order. However, the CEF-RKKY competition is still responsible for complex magnetic ground states, and it appears that the electronic and magnetic degrees of freedom are entangled in all magnetic members of this series of compounds.

DOI: [10.1103/PhysRevMaterials.5.094416](https://doi.org/10.1103/PhysRevMaterials.5.094416)

I. INTRODUCTION

Rare earth (R) intermetallic compounds have garnered a lot of interest in condensed matter systems due to their wide range of properties, such as unconventional superconductivity [1–3], Kondo behavior [4–6], and quantum criticality [7–9], through the interplay between magnetic interactions, the Kondo effect, and crystal electric field (CEF) anisotropy [10]. While the Kondo effect occurs mostly in Ce- and Yb-based compounds [11–14], Ruderman-Kittel-Kasuya-Yosida (RKKY) interactions and CEF effects are ubiquitous in magnetic intermetallics. These competing interactions (RKKY, CEF, Kondo) not only break the ground state CEF degeneracy and result in magnetic anisotropy, but also can result in unconventional magnetic order [15,16].

Currently, several Kondo systems based on both Ce and Yb rare earths, $YbNi_4P_2$ [17], $CeRuPO$ [18], $CeAgSb_2$ [19] and Co-doped $YbRh_2Si_2$ [20], have been shown to display complex magnetic ground state, where the moments ordered along the hard CEF axis. Such hard axis ordering in Kondo lattice systems [21–23] has been observed independent of the crystal symmetry [17–19], ordered moment size [24–26], or Kondo temperature scale T_K relative to the ferromagnetic

ordering temperature T_C [17,18,27]. While this property was initially thought to be a result of electronic particle-hole fluctuations in ferromagnetic heavy fermion compounds [28], we recently discovered similar hard axis order in both ferro- (FM) and antiferro-magnetic (AFM) Kondo systems, in three isostructural Yb compounds, $YbIr_3Ge_7$ [29], $YbRh_3Si_7$ [30], and $YbIr_3Si_7$ [31]. These observations on Kondo and non-Kondo magnetic systems lead to new questions: what is the exact mechanism for the hard axis ordering, and what are the roles of each of the competing energy scales, RKKY, CEF and Kondo, in driving the hard axis ordering?

The most suitable strategy is to deconvolute the effect of each interaction. To this end, we performed a systematic study of the magnetic and electronic properties of isostructural RRh_3Si_7 compounds, where only RKKY interactions are present in the $R = Gd$ member, RKKY and CEF effects compete in the $R = Tb-Tm$ systems, while all three energy scales (RKKY, CEF, Kondo) are present in the $R = Yb$ compound. For a more in-depth comparison, we took advantage of our recent discovery of isostructural Kondo systems $YbIr_3Ge_7$ [29], $YbRh_3Si_7$ [30] and $YbIr_3Si_7$ [31], a rare example of Kondo analogs with the same crystal symmetry and similar lattice parameters. Our results show, as expected, that the least magnetic anisotropy is present in $GdRh_3Si_7$ with orbital angular momentum $L = 0$. In RRh_3Si_7 where $R = Tb-Tm$, we find that the CEF interaction strength varies and leads to

*emorosan@rice.edu

a ground state magnetic anisotropy change from easy plane (up to $R = \text{Tb-Ho}$) to easy axis ($R = \text{Er, Tm}$) ordering. It is only when $R = \text{Yb}$, where all three types of interactions are present, that hard axis magnetic ordering occurs for all three Kondo compounds YbRh_3Si_7 , YbIr_3Ge_7 and YbIr_3Si_7 . These findings reaffirm the dominant role of strong correlations in the presence of CEF effects that drive the hard axis long-range magnetic order. In addition, our study reveals a breakdown of the expected de Gennes scaling [32] of the magnetic ordering temperature in the RRh_3Si_7 series, with the $R = \text{Yb}$ showing the highest ordering temperature at 7.5 K, and extremely low ordering temperatures in the $R = \text{Tb, Ho, and Er}$ compounds ($< 0.5 \text{ K}$).

II. METHODS

Single crystals of RRh_3Si_7 ($R = \text{Gd-Tm}$) have been grown from a Rh-Si liquid solution, similar to the growth of YbRh_3Si_7 [30]. The resulting crystals (shown in the inset, Fig. 1) have typical dimensions of $6 \times 6 \times 4 \text{ mm}^3$. The powder x-ray diffraction (XRD) measurements were performed in a Bruker D8 diffractometer with $\text{Cu K}\alpha$ radiation. The Rietveld structural refinement was achieved by the TOPAS software. Single crystal XRD measurements were performed on Bruker D8 Quest Kappa diffractometer equipped with an $I\mu\text{S}$ microfocuss source ($\text{Mo K}\alpha$, $\lambda = 0.71073 \text{ \AA}$), a HELIOS optics monochromator, and a PHOTON II CPAD detector.

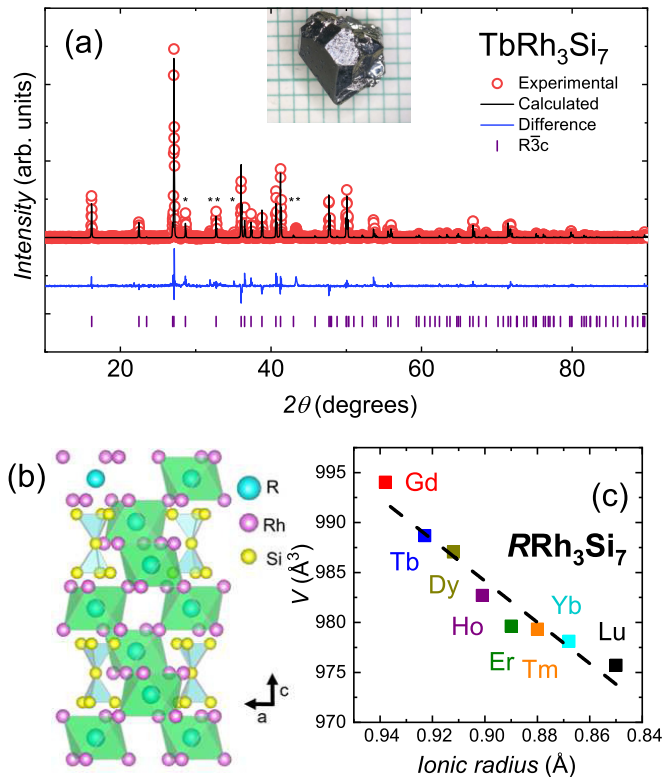


FIG. 1. (a) Powder x-ray diffraction (symbols) and Rietveld refinement (black line) at 300 K for TbRh_3Si_7 , with an image of a TbRh_3Si_7 crystal in the inset. (b) Crystal structure of RRh_3Si_7 ($R = \text{Gd-Tm}$). (c) Unit cell volume V vs ionic radius of R^{3+} for RRh_3Si_7 ($R = \text{Gd-Lu}$), with the dashed line showing the expected lanthanide contraction [34].

The integration of the diffraction data was performed using the Bruker SAINT program and the absorption correction was done using the Bruker program SADABS2016/2 (multi-scan method). Structure models were generated using intrinsic phasing methods in SHELXT program, and anisotropically refined using SHELXL2014 program. The LuRh_3Si_7 compound was synthesized in polycrystalline form by arc-melting stoichiometric amounts of the constituent elements [30].

DC magnetization measurements were performed in a Quantum Design Magnetic Property Measurement System (QD) with a ^3He option. Specific heat measurements were carried out in a QD Physical Property Measurement System with a ^3He option. Resistivity was measured in a four-point contact geometry in a Dynacool with electrical transport option with AC current with frequency of 9.1 Hz and driving amplitude of 1 mA.

III. RESULTS

A. Structural characterization

RRh_3Si_7 belong to the ScRh_3Si_7 class of compounds, which crystallizes in a rhombohedral structure with space group: $R\bar{3}c$ [33]. A representative powder XRD data is shown in Fig. 1(a) for TbRh_3Si_7 . The Rietveld refinement confirms the $R\bar{3}c$ crystal structure, with a few minute impurity peaks [marked by “*” in Fig. 1(a)] due to small amounts of remnant Rh-Si flux, while small intensity differences between measured (red circles) and calculated (black line) patterns may be due to preferred orientation. The structure, stoichiometry, crystal purity, and orientation of the crystals are also confirmed by single crystal XRD. The RRh_3Si_7 structure is comprised of Si_7 bipyramids [light blue, Fig. 1(b)] and RRh_6 octahedra (green). The lattice parameters of RRh_3Si_7 obtained from powder crystal XRD are summarized in Table I. The unit cell volume decreases linearly with the ionic radius of R^{3+} , which is in line with the expected lanthanide contraction [Fig. 1(c)].

B. Temperature-dependent magnetization

The low-temperature magnetic susceptibility M/H , measured with an applied field $\mu_0 H = 0.1 \text{ T}$ parallel to the a and c axes of the equivalent hexagonal unit cell, are shown in Fig. 2. For $R = \text{Gd}$ and Dy , a peak is observed below $T = 5$ and 2.5 K , respectively, likely due to long-range antiferromag-

TABLE I. Lattice parameters of RRh_3Si_7 ($R = \text{Gd-Lu}$) determined from powder x-ray diffraction refinements.

R in RRh_3Si_7	a (\AA)	c (\AA)	unit cell volume (\AA^3)
Gd	7.596	19.891	994.04
Tb	7.583	19.853	988.69
Dy	7.574	19.866	987.05
Ho	7.566	19.822	982.70
Er	7.555	19.817	979.64
Tm	7.552	19.827	979.34
Yb [30]	7.548	19.823	978.13
Lu [30]	7.542	19.806	975.72

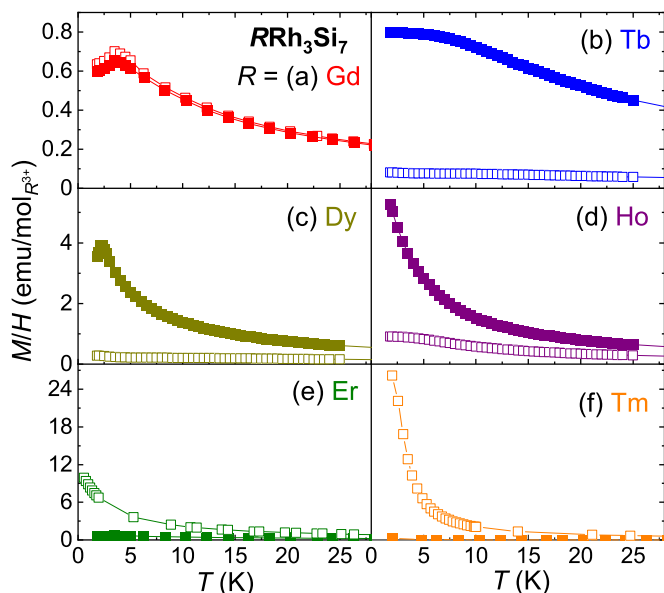


FIG. 2. Temperature-dependent magnetic susceptibility with $\mu_0 H = 0.1 T$ for $H \parallel a$ (full symbols) and $H \parallel c$ (open symbols) of RRh_3Si_7 ($R = Gd-Tm$).

netic order [Figs. 2(a), (c)]. For $R = Ho$, Er and Tm, M/H increases monotonically upon cooling, with no obvious sign of magnetic order down to the lowest measured temperature of $T = 1.8 K$ [Figs. 2(d)–2(f)]. The susceptibility for the Tb compound plateaus at the lowest temperatures [Fig. 2(b)], where a broad peak in the specific heat (discussed below) signals possible short-range correlations.

The inverse average magnetic susceptibility H/M_{ave} is shown in Fig. 3, where the average magnetization M_{ave} is calculated as $M_{ave} = (2M_a + M_c)/3$. For $R = Gd-Ho$, H/M_{ave} follows a Curie-Weiss behavior as $H/M_{ave} = (T - \theta_W)/C$,

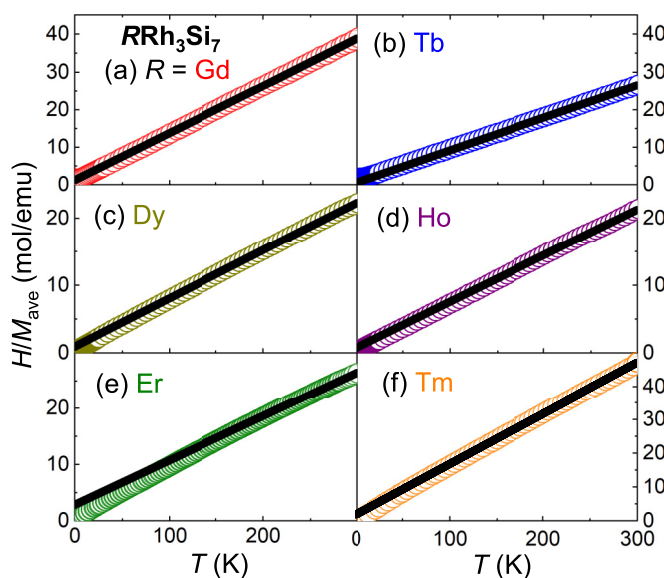


FIG. 3. Inverse magnetic susceptibility H/M_{ave} (symbols) of RRh_3Si_7 ($R = Gd-Tm$) for $\mu_0 H = 0.1 T$. Solid lines are Curie-Weiss fits.

where θ_W is the Weiss temperature and C is the Curie constant, between $T = 300$ and $50 K$, as shown by the solid black lines in Fig. 3. For $R = Er$ and Tm, deviations from Curie-Weiss behavior are observed starting at higher temperatures, at around $150 K$. From the linear fit at high temperatures, the effective magnetic moment μ_{eff} obtained for all compounds is consistent with R^{3+} state, while the negative Weiss temperatures θ_W point to antiferromagnetic correlations across the series. Table II summarizes θ_W , μ_{eff}^{th} , μ_{eff}^{exp} , the ordering temperature T_{ord} as well as the de Gennes factor $dG = (g_J - 1)^2 J(J + 1)$, a scaling parameter for the ordering temperature (discussed below).

The magnetic susceptibility shown in Fig. 2 indicates easy plane anisotropy for $R = Tb-Ho$, and a switch to easy axis for $R = Er-Tm$. This is similar to what had been observed in other intermetallic series with tetragonal ($RAgSb_2$ [19]) or orthorhombic ($RAgGe$ [35], $RPtIn$ [36]) point symmetry, where the switch of magnetic order from easy plane to easy axis was understood within a simplified uniaxial anisotropy picture [37]: the B_{20} Stevens coefficient switches from positive to negative in moving from light to heavier R , and is nearly 0 for the $R = Ho$ and Er compounds in the series. Such a mechanism appears to apply to RRh_3Si_7 despite the trigonal point symmetry of the magnetic site, such that $HoRh_3Si_7$ has the smallest anisotropy as $M_a/M_c \leq 5$ in the paramagnetic state [Fig. 2(d)].

C. Field-dependent magnetization

The RRh_3Si_7 $M(H)$ isotherms measured at $T = 1.8 K$ (Fig. 4) are consistent with the anisotropy revealed by the temperature-dependent magnetization data. Not surprisingly, the $H \parallel a$ (full symbols) and $H \parallel c$ (open symbols) $M(H)$ curves for $GdRh_3Si_7$ [Fig. 4(a)] are nearly identical, and saturate at $7\mu_B$ when $\mu_0 H = 7 T$, in line with the Gd^{3+}

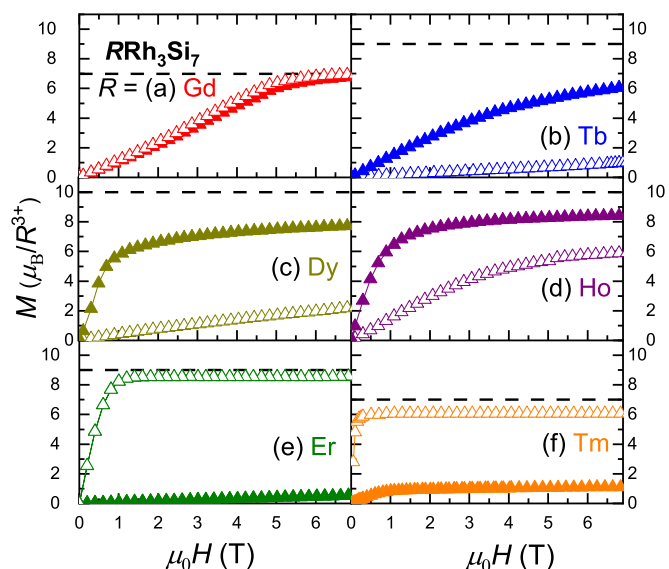


FIG. 4. Field-dependent magnetization measured at $T = 1.8 K$ for $H \parallel a$ (full symbols) and $H \parallel c$ (open symbols) for RRh_3Si_7 ($R = Gd-Tm$). Horizontal dashed lines indicate the saturated moments of the R^{3+} ions calculated from Hund's rules.

TABLE II. Magnetic and transport properties of RRh_3Si_7 compounds. θ_W is the Curie-Weiss temperature, $\mu_{\text{eff}}^{\text{th}}$ and $\mu_{\text{eff}}^{\text{exp}}$ are the theoretical and experimental effective moment values for R^{3+} , respectively. dG is the de Gennes factor $dG = (g_J - 1)^2 J(J + 1)$, T_{ord} is the magnetic ordering temperature, and T^* is the CEF temperature where a broad peak is observed in C_m for $R = \text{Tb, Dy, and Ho}$. $RRR = \rho_{300\text{K}}/\rho_{2\text{K}}$ is the residual resistivity ratio.

R in RRh_3Si_7	θ_W (K)	$\mu_{\text{eff}}^{\text{th}} (\mu_B)$	$\mu_{\text{eff}}^{\text{exp}} (\mu_B)$	dG	$T_{\text{ord}}(\text{K}), T^*(\text{K})$	RRR
Gd	-9.7	7.94	7.97	15.75	3.4	14
Tb	-5.1	9.72	9.56	10.50	<0.062, 11.7	27
Dy	-13.3	10.65	10.58	7.08	2.0, 13.9	17
Ho	-10.2	10.61	10.78	4.50	0.11, 2.2	14
Er	-23.3	9.58	9.9	2.55	0.46	8
Tm	-13.8	7.94	7.33	1.17	3.2	6
Yb [30]	-26.5	4.54	4.1	0.32	7.5	0.96

ground state $J = 7/2$ multiplet. For $R = \text{Tb, Dy, and Ho}$, the magnetization fails to reach the theoretical saturation value, $\mu_{\text{sat}} = 9, 10, 10 \mu_B$, respectively, at $\mu_0 H = 7 T$. This result confirms that CEF splits the ground state multiplet, with easy plane ordering, since $M_a = M(H \parallel a) > M(H \parallel c) = M_c$, consistent with the high T magnetic susceptibility data (Fig. 2). The ratio of the saturated magnetization between the two field directions, $(M_a/M_c)_{7T}$, decreases in moving across the series from light to heavy rare earths. In the case of $R = \text{Er}$ and Tm , the anisotropy switches, and it is M_c that plateaus at fields above $\sim 1-2 T$ [open symbols, Figs. 4(d) and 4(f)], while M_a remains very small ($\leq 1 \mu_B$) for the entire measured field range. This is consistent with an easy CEF axis along the c crystallographic direction based on the high temperature susceptibility measurements [Figs. 2(e)-2(f)].

D. Specific heat measurements

Figure 5 shows temperature-dependent specific heat measurements. Sharp peaks in $C_p(T)$ indicate long-range magnetic order in RRh_3Si_7 with $R = \text{Gd, Dy, Ho, Er, and Tm}$. TbRh_3Si_7 shows sign of long-range magnetic order just below 0.062 K. For $R = \text{Tb, Dy, and Ho}$, additional broad C_p peaks are observed above T_{ord} , at temperatures denoted as T^* listed in Table II. As discussed below, the broad specific heat peaks are likely associated with CEF splitting, consistent with the departures from Curie-Weiss behavior observed in the average inverse susceptibilities (Fig. 3).

We further estimate the magnetic entropy S_m from the specific heat data by subtracting the values for the nonmagnetic analog LuRh_3Si_7 . The magnetic specific heat C_m for RRh_3Si_7 ($R = \text{Gd-Tm}$) is evaluated as $C_m = C_p(RRh_3Si_7) - C_p(\text{LuRh}_3Si_7)$, and the magnetic entropy is calculated from $S_m = \int \frac{C_m}{T} dT$. The results are shown in Fig. 6. The arrows mark the ordering temperature for each compound, except TbRh_3Si_7 whose magnetic ordering temperature is just below the minimum measured temperature 0.062 K. The magnetic entropy at T_{ord} in GdRh_3Si_7 is close to $R \ln 8$, indicating an eightfold degenerate ground state as expected for its $J = 7/2$ ground state. For the rest of RRh_3Si_7 , the magnetic entropy release at T_{ord} is less than $R \ln(2J + 1)$, which indicates the presence of excited CEF levels. Further inelastic neutron

scattering measurements are required to clarify the exact CEF configurations in each compound.

E. Resistivity measurements

The electrical resistivities $\rho(T)$ of the RRh_3Si_7 ($R = \text{Gd-Tm}$) compounds show metallic behavior, with ρ decreasing on cooling (Fig. 7). The complex anisotropic magnetic properties of the RRh_3Si_7 compounds can therefore be attributed to the competition between CEF effects and RKKY interactions, as expected in metallic systems [38]. Following the linear decrease of $\rho(T)$ from room temperature, a drop in the resistivity is observed for $R = \text{Gd, Dy, and Tm}$ below T_{ord} [inset, Figs. 7(a)-7(f)], consistent with loss of spin disorder scattering. In comparison, the low- T resistivity in ErRh_3Si_7 remains nearly temperature independent down to 1.8 K, consistent with the lack of magnetic ordering above this temperature. The residual resistivity ra-

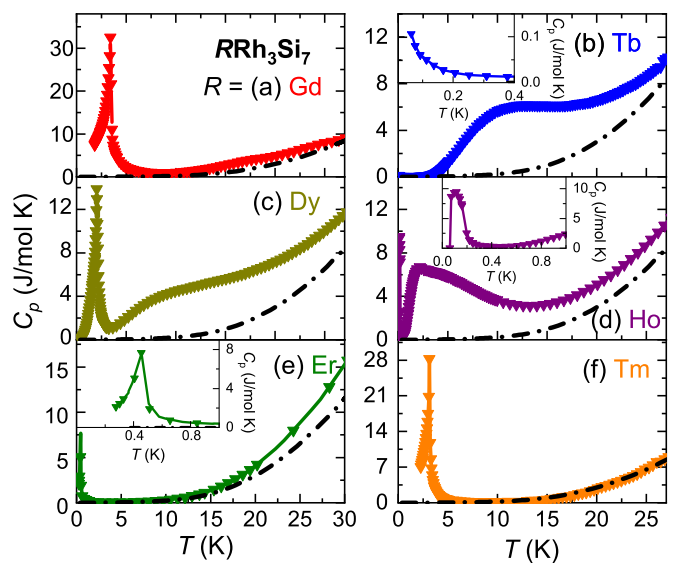


FIG. 5. Zero-field specific heat for RRh_3Si_7 . The insets in (b), (d), and (e) show the lower temperature range of the corresponding specific heat curve. The dashed line indicates the specific heat of the nonmagnetic analog LuRh_3Si_7 .

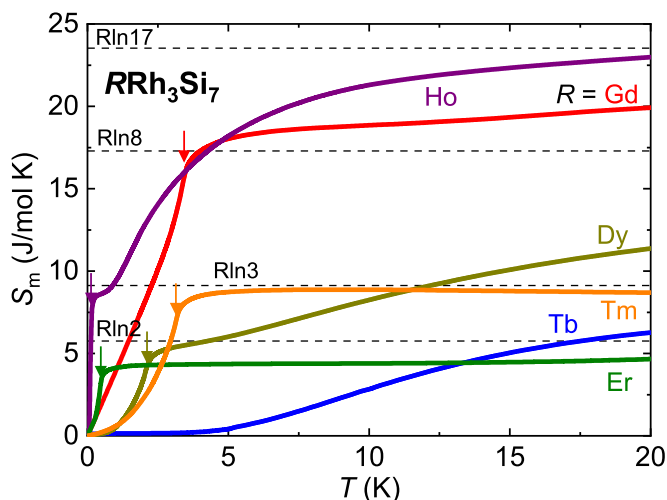


FIG. 6. Magnetic entropy S_m for RRh_3Si_7 ($R = \text{Gd-Tm}$). The vertical arrows indicate the ordering temperatures defined by the sharp peak in specific heat measurement, as discussed in the main text.

tion RRR , defined as $RRR = \rho_{300K}/\rho_{2K}$, is between 6 (for $R = \text{Tm}$) and 27 (for $R = \text{Tb}$) (Table II), suggesting overall good crystal quality. An unexpected upturn in $\rho(T)$ occurs on cooling just above the magnetic ordering temperatures, in the $R = \text{Gd}$, Dy , and possibly Tm members of the series. This feature will be revisited in the Discussion section.

The semilog plot in Fig. 7(g) compares the normalized resistivities of all RRh_3Si_7 , including the Kondo antiferromagnet $R = \text{Yb}$ (light blue triangle) and the non-magnetic $R = \text{Lu}$ (dashed line), together with those of the isostructural compounds YbIr_3Ge_7 (purple hexagon) and YbIr_3Si_7 (blue star). The resistivity of LuRh_3Si_7 is metallic, in line with the values of the other compounds in this series. In stark contrast, the three Yb compounds stand out as a poor or low-carrier metals [29,30] or insulator [31]. While YbIr_3Ge_7 (purple hexagon) appears metallic, it shows a weak temperature dependence. The resistivity for YbRh_3Si_7 (light blue triangle) increases on cooling and yields a local maximum associated with Kondo resonance around 20 K. A nearly four orders of magnitude increase in $\rho(T)$ is apparent in YbIr_3Si_7 (dark blue star), which we rationalized elsewhere [31] within a Kondo exhaustion scenario.

IV. DISCUSSION

Our thermodynamic and electrical transport data reveal CEF anisotropy, magnetic ordering below T_{ord} and metallic behavior for the RRh_3Si_7 compounds with $R = \text{Gd-Tm}$. In most R -based intermetallic series, mean-field theory based on RKKY interaction predicts the scaling of the magnetic ordering temperature with the de Gennes factor $dG = (g_J - 1)^2 J(J + 1)$, where g_J is the Lande g factor and J is the total angular momentum of the ground-state multiplet dictated by the Hund's rule for R^{3+} . This prediction holds unless frustration and other unconventional effects exist. In RRh_3Si_7 ($R = \text{Gd-Yb}$), Table II indicates a nonmonotonous change of T_{ord} across the series, leading to the breakdown of de Gennes

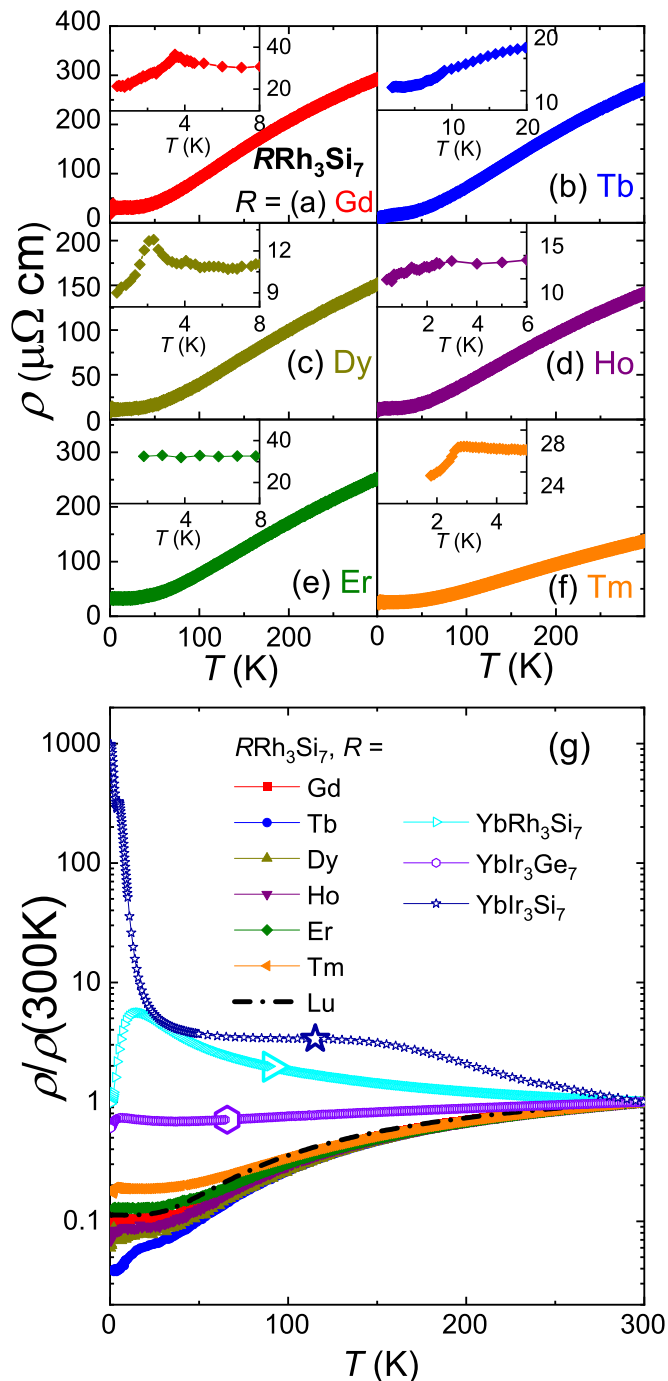


FIG. 7. (a)–(f) Zero-field resistivity for RRh_3Si_7 ($R = \text{Gd-Tm}$) with $i \parallel c$. (g) Semilog plot of the normalized resistivity $\rho/\rho(300\text{K})$ for RRh_3Si_7 , including the data for $R = \text{Yb}$ (light blue) and Lu (dashed line)[30], and the respective curves for the isostructural Kondo compounds YbIr_3Ge_7 [29] and YbIr_3Si_7 [12].

scaling: all compounds with $R = \text{Gd-Tm}$ order below 3.4 K. While GdRh_3Si_7 has the highest T_{ord} at 3.4 K, it is still much lower than the T_{ord} of YbRh_3Si_7 at 7.5 K, even in the absence of CEF interaction in the former compound. Extremely low ordering temperatures $T_{\text{ord}} < 0.5$ K are observed in some members of the series ($R = \text{Tb}$, Ho , and Er). All compounds except GdRh_3Si_7 show clear magnetic anisotropy, and the

saturated magnetization values are less than the theoretical μ_{sat} for $R = \text{Tb-Ho}$, which suggests canted moments in the ordered state, or metamagnetic transitions at higher fields, or both. The anisotropy decreases from light to heavy R , resulting in a nearly isotropic HoRh_3Si_7 [Fig. 4(d)]. This trend fits within a simplified uniaxial anisotropy model [37], where the B_{20} Stevens coefficient decreases down to nearly 0 ($R = \text{Ho}$) in moving from light to heavier R . For even heavier R , the anisotropy changes from easy plane to easy axis when $R = \text{Er, Tm}$, and their c axis magnetization reaches the expected saturation value at $\mu_0 H = 7 T$.

The specific heat data reveals the presence of CEF effects, with low lying energy levels in the $R = \text{Tb, Dy}$, and Ho compounds, indicated by a broad peak around T^* in C_p (Fig. 5). Additionally, the magnetic entropy S_m is less than $R \ln(2J + 1)$ at the respective magnetic ordering temperature for all RRh_3Si_7 (Fig. 6). GdRh_3Si_7 is the exception, since no CEF anisotropy is expected for $L = 0$, as is the case for Gd^{3+} . In rare earth intermetallic systems, a broad maximum in C_p and a reduced entropy at their magnetic ordering temperature [Figs. 5(b), (d)] could be either due to the existence of low-lying CEF levels or Kondo effects, or both. Usually, the Kondo effect is weak, if not absent, in the f -electron systems with more than one electron or hole in the f shell. Therefore, the broad C_p peaks and the reduced S_m in $R = \text{Tb, Dy}$ and Ho could only be attributed to CEF splitting of the ground state multiplet together with possible short-range correlations at higher temperatures. The same mechanism can be applied to the smaller magnetic entropy ($< R \ln(2J + 1)$), which appears in $R = \text{Tm}$ and Er .

While less affected by CEF, the electrical resistivities of the RRh_3Si_7 compounds underscore the RKKY coupling, which contributes to the complex energy competition in this series. All the non-Kondo RRh_3Si_7 compounds are good metals, showing linear decrease of $\rho(T)$ on cooling, and signatures of spin disorder scattering at T_{ord} when it is in the measured temperature range (Fig. 7). An unexpected upturn in $\rho(T)$ precedes the magnetic order in the $R = \text{Gd, Dy}$, and possibly Tm members of the series. This is a rare occurrence in intermetallic compounds: such a peak in $\rho(T)$ at T_{ord} was attributed to a pseudogap formation in CeAgAs_2 [39], or enhanced spin fluctuations due to spin wave excitations in MnBi_2Te_4 [40] and Fe_{1+y}Te [41]. Another possible explanation is a small structural distortion associated with the magnetic order. Other plausible albeit less likely scenarios are a density wave formation, where the removal of states from the Fermi surface competes with the loss of spin disorder scattering, or Kondo screening. Band structure calculations will be necessary to verify the possible pseudogap formation, while low temperature (below T_{ord}) structural analysis is required to evaluate any structural distortions. Low temperature neutron scattering could shed light on the possibility of spin wave excitations and the interaction of the local moments with the itinerant carriers.

Once we turn to the Kondo compounds in our comparison (YbIr_3Si_7 , YbIr_3Ge_7 and YbRh_3Si_7) several observations come to fore: their normalized resistivity at low temperature [open symbols in Fig. 7(g)] is much larger than that of the non-Kondo compounds in this structure; the low-temperature magnetic susceptibility data (Fig. 8) show a crossover on cooling below 12 K, indicating hard-CEF axis magnetic order.

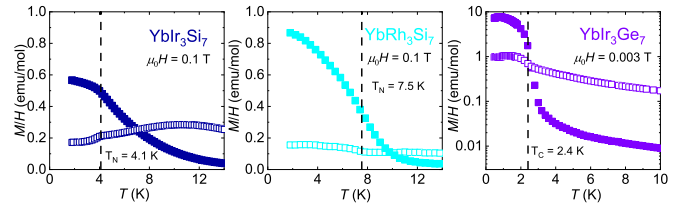


FIG. 8. Hard axis ordering of YbIr_3Si_7 , YbIr_3Ge_7 and YbRh_3Si_7 . $H \parallel a$ (full symbols) and $H \parallel c$ (open symbols). The dashed lines indicate the magnetic ordering temperature.

The relative energy scales of the three interactions in RRh_3Si_7 family can be estimated in the following way: The RKKY energy should be $\sim 0-10$ K, close to the magnetic ordering temperatures (listed in Table II). Note that for this series of compounds, the magnetic ordering temperatures are consistently smaller than the Curie-Weiss temperatures, particularly for $R = \text{Tb, Ho}$, and Er where T_{ord} is below 0.5 K, implying a certain degree of frustration. Meanwhile, the CEF energy scale Δ can be estimated from hard-axis magnetic susceptibility, to be further confirmed by neutron experiments [42,43]. For most RRh_3Si_7 ($R = \text{Tb-Tm}$), Δ appears to be in the range of $\sim 10-50$ K based on the hard axis temperature-dependent magnetic susceptibility data and the broad peak in specific heat data, and likely higher than 300 K only for $R = \text{Yb}$. These values are common for R -based intermetallics [44]. However, the exact CEF splitting in the series of RRh_3Si_7 compounds, with the R in a trigonal point symmetry, is more difficult to pinpoint (see, for example, our detailed study of the CEF splitting in an isostructural compound CeIr_3Ge_7 [42,43]) and this is beyond the scope of the current study. At last, the Kondo energy was estimated to be around 15 K for YbRh_3Si_7 [30].

While YbRh_3Si_7 with all three interactions shows magnetic crossing in the low- T magnetization (Fig. 8) for the two field directions, no such crossover appears (Fig. 2) for the non-Kondo systems RRh_3Si_7 ($R = \text{Gd-Tm}$). These results point to the Kondo effect as an essential ingredient for the formation of hard-axis magnetic ordering in the YbRh_3Si_7 and the other Kondo analogs. Beyond the anisotropy, the interplay of Kondo and CEF is also remarkable considering that YbRh_3Si_7 shows nearly record-high ordering temperature $T_N \sim 8$ K, with the other two Kondo compounds YbIr_3Si_7 and YbIr_3Ge_7 also having larger T_{ord} than what is often observed in Yb heavy-fermion compounds [45-47]. This recalls the possibility of yet another relevant scale, spin-orbit coupling (SOC), playing a role, given that Ir is much heavier than (while otherwise chemically quite similar to) its $4d$ analog Rh . Detailed spectroscopy experiments are required to elucidate the correlation-SOC interplay, and these are underway.

V. CONCLUSIONS

In summary, we have successfully synthesized single crystals of the novel intermetallic compounds RRh_3Si_7 ($R = \text{Gd-Tm}$). We investigate their thermodynamic and electrical properties by contrast to three Kondo isostructural systems YbIr_3Si_7 , YbIr_3Ge_7 , and YbRh_3Si_7 , to understand the respective roles of CEF, RKKY, and Kondo interactions towards

hard-axis magnetic ordering. Such a comparison suggests that the Kondo effect is the main mechanism behind the hard axis ordering. In addition, the abnormally high magnetic ordering temperature in the three Kondo systems mark the competition between three energy scales (and possibly SOC) in the systems. When the Kondo effect is removed, the competition between RKKY and CEF is reflected in the magnetic ordering temperatures, which do not follow the expected de Gennes scaling (Table II). Furthermore, the $R = \text{Tb}$, Ho , and Er members of this series have extremely low T_{ord} below 0.5 K. The resistivity measurements reveal that all the non-Kondo $RRh_3\text{Si}_7$ compounds are good metals, and show signs of spin disorder scattering at T_{ord} , although an unexpected upturn occurs before the T_{ord} in $R = \text{Gd}$, Dy , and possibly Tm . This can be caused by multiple mechanisms and can be verified using approaches such as band structure calculations or low temperature neutron diffraction. When CEF is removed

and only the RKKY effect is at play, which is the case in GdRh_3Si_7 , the magnetic properties become relatively simple, and no apparent magnetic anisotropy is observed. From light to heavy R , decreasing CEF anisotropy is observed, and this ultimately makes the anisotropy change from easy plane to easy axis for $R = \text{Er}$, Tm , with the latter two compounds reaching saturation at low fields ($\sim 1\text{--}2$ T).

ACKNOWLEDGMENTS

L.Q., S.L., C.-L.H. and E.M. acknowledge support from U.S. Department of Energy (DOE) BES DE-SC0019503. J.Y.C. acknowledges support from the National Science Foundation under Grant No. DMR-1700030. A.M.H acknowledges support from the the Natural Sciences and Engineering Research Council of Canada and the CIFAR Azrieli Global Scholars program.

-
- [1] F. Steglich, J. Aarts, C. D. Bredl, W. Lieke, D. Meschede, W. Franz, and H. Schäfer, *Phys. Rev. Lett.* **43**, 1892 (1979).
- [2] N. D. Mathur, F. M. Grosche, S. R. Julian, I. R. Walker, D. M. Freye, R. K. W. Haselwimmer, and G. G. Lonzarich, *Nature (London)* **394**, 39 (1998).
- [3] C. Petrovic, R. Movshovich, M. Jaime, P. G. Pagliuso, M. F. Hundley, J. L. Sarrao, Z. Fisk, and J. D. Thompson, *Europhys. Lett.* **53**, 354 (2001).
- [4] J. Stankiewicz, M. Evangelisti, Z. Fisk, P. Schlottmann, and L. P. Gor'kov, *Phys. Rev. Lett.* **108**, 257201 (2012).
- [5] M. H. Jung, A. H. Lacerda, and T. Takabatake, *Phys. Rev. B* **65**, 132405 (2002).
- [6] L. Menon and S. K. Malik, *Phys. Rev. B* **51**, 5858 (1995).
- [7] G. Giovannetti, S. Kumar, and J. van den Brink, *Phys. B* **403**, 3653 (2008).
- [8] C. Liu, V. F. C. Humbert, T. M. Bretz-Sullivan, G. Wang, D. Hong, F. Wrobel, J. Zhang, J. D. Hoffman, J. E. Pearson, J. S. Jiang, C. Chang, A. Suslov, N. Mason, M. R. Norman, and A. Bhattacharya, *Nat. Commun.* **11**, 1402 (2020).
- [9] D. Das, D. Gnida, P. Wiśniewski, and D. Kaczorowski, *Proc. Natl. Acad. Sci. USA* **116**, 20333 (2019).
- [10] G. R. Stewart, *Rev. Mod. Phys.* **73**, 797 (2001).
- [11] A. T. Boothroyd, J. P. Barratt, P. Bonville, P. C. Canfield, A. Murani, A. R. Wildes, and R. I. Bewley, *Phys. Rev. B* **67**, 104407 (2003).
- [12] J. P. Sanchez and M. M. Abd-Elmeguid, *Hyperfine Interact.* **128**, 137 (2000).
- [13] S. Seiro, L. Jiao, S. Kirchner, S. Hartmann, S. Friedemann, C. Krellner, C. Geibel, Q. Si, F. Steglich, and S. Wirth, *Nat. Commun.* **9**, 3324 (2018).
- [14] G. Poelchen, S. Schulz, M. Mende, M. Güttler, A. Generalov, A. V. Fedorov, N. Caroca-Canales, C. Geibel, K. Kliemt, C. Krellner, S. Danzenbächer, D. Y. Usachov, P. Dudin, V. N. Antonov, J. W. Allen, C. Laubschat, K. Kummer, Y. Kucherenko, and D. V. Vyalikh, *npj Quantum Mater.* **5**, 70 (2020).
- [15] J. C. G. Sal, J. I. E. Martínez, J. R. Fernández, N. M. Aguado, A. Señas, J. García Soldevilla, and J. Blanco, *Iran. J. Phys. Res.* **8**, 73 (2008).
- [16] A. Szytuła, *Mater. Sci. Poland* **24**, 737 (2006).
- [17] A. Steppke, R. KÜchler, S. Lausberg, E. Lengyel, L. Steinke, R. Borth, T. Lühmann, C. Krellner, M. Nicklas, C. Geibel, F. Steglich, and M. Brando, *Science* **339**, 933 (2013).
- [18] C. Krellner and C. Geibel, *J. Cryst. Growth* **310**, 1875 (2008).
- [19] K. Myers, S. Bud'ko, I. Fisher, Z. Islam, H. Kleinke, A. Lacerda, and P. Canfield, *J. Magn. Magn. Mater.* **205**, 27 (1999).
- [20] S. Lausberg, A. Hannaske, A. Steppke, L. Steinke, T. Gruner, L. Pedrero, C. Krellner, C. Klingner, M. Brando, C. Geibel, and F. Steglich, *Phys. Rev. Lett.* **110**, 256402 (2013).
- [21] D. Hafner, B. K. Rai, J. Banda, K. Kliemt, C. Krellner, J. Sichelschmidt, E. Morosan, C. Geibel, and M. Brando, *Phys. Rev. B* **99**, 201109(R) (2019).
- [22] M. Kasaya, T. Tani, K. Kawate, T. Mizushima, Y. Isikawa, and K. Sato, *J. Phys. Soc. Jpn.* **60**, 3145 (1991).
- [23] K. Katoh, S. Nakagawa, G. Terui, and A. Ochiai, *J. Phys. Soc. Jpn.* **78**, 104721 (2009).
- [24] Y. Muro, Y. Haizaki, M. S. Kim, K. Umeo, H. Tou, M. Sera, and T. Takabatake, *Phys. Rev. B* **69**, 020401(R) (2004).
- [25] K. Umeo, H. Yamane, H. Kubo, Y. Muro, F. Nakamura, T. Suzuki, T. Takabatake, K. Sengupta, M. K. Forthaus, and M. M. Abd-Elmeguid, *Phys. Rev. B* **85**, 024412 (2012).
- [26] N. Tsujii, L. Keller, A. Dönni, and H. Kitazawa, *J. Phys.: Condens. Matter* **28**, 336002 (2016).
- [27] V. Fritsch, O. Stockert, C.-L. Huang, N. Bagrets, W. Kittler, C. Taubenheim, B. Pilawa, S. Woitschach, Z. Huesges, S. Lucas, A. Schneidewind, K. Grube, and H. V. Löhneysen, *Eur. Phys. J.: Spec. Top.* **224**, 997 (2015).
- [28] F. Krüger, C. J. Pedder, and A. G. Green, *Phys. Rev. Lett.* **113**, 147001 (2014).
- [29] B. K. Rai, M. Stavinoha, J. Banda, D. Hafner, K. A. Benavides, D. A. Sokolov, J. Y. Chan, M. Brando, C.-L. Huang, and E. Morosan, *Phys. Rev. B* **99**, 121109(R) (2019).
- [30] B. K. Rai, S. Chikara, X. Ding, I. W. H. Oswald, R. Schönemann, V. Loganathan, A. M. Hallas, H. B. Cao, M. Stavinoha, T. Chen, H. Man, S. Carr, J. Singleton, V. Zapf, K. A.

- Benavides, J. Y. Chan, Q. R. Zhang, D. Rhodes, Y. C. Chiu, L. Balicas *et al.*, *Phys. Rev. X* **8**, 041047 (2018).
- [31] M. Stavinoha, C. L. Huang, W. A. Phelan, A. M. Hallas, V. Loganathan, J. W. Lynn, Q. Huang, F. Weickert, V. Zapf, K. R. Larsen, P. D. Sparks, J. C. Eckert, A. B. Puthirath, C. Hooley, A. H. Nevidomskyy, and E. Morosan, [arXiv:1908.11336](https://arxiv.org/abs/1908.11336).
- [32] G. Drachuck, A. E. Böhmer, S. L. Bud'ko, and P. C. Canfield, *J. Magn. Magn. Mater.* **417**, 420 (2016).
- [33] B. Chabot, N. Engel, and E. Parthé, *Acta Crystallographica Section B* **37**, 671 (1981).
- [34] A. G. Sharpe and C. E. Housecroft, *Inorganic Chemistry*, 2nd ed. (Prentice Hall, NJ, 2004), pp. 536.
- [35] E. Morosan, S. Bud'ko, P. Canfield, M. Torikachvili, and A. Lacerda, *J. Magn. Magn. Mater.* **277**, 298 (2004).
- [36] E. Morosan, S. L. Bud'ko, and P. C. Canfield, *Phys. Rev. B* **72**, 014425 (2005).
- [37] K. N. R. Taylor and M. I. Darby, *Physics of Rare Earth Solids* (Chapman and Hall, London, 1972), p. 22.
- [38] A. Kumar, P. K. Ahluwalia, S. Kumar, and K. C. Sharma, *Phys. Rev. B* **56**, 3145 (1997).
- [39] R. Mondal, R. Bapat, S. K. Dhar, and A. Thamizhavel, *Phys. Rev. B* **98**, 115160 (2018).
- [40] M. M. Otrokov, I. I. Klimovskikh, H. Bentmann, D. Estyunin, A. Zeugner, Z. S. Aliev, S. Gaß, A. U. B. Wolter, A. V. Koroleva, A. M. Shikin, M. Blanco-Rey, M. Hoffmann, I. P. Rusinov, A. Vyazovskaya, S. V. Ereemeev, Y. M. Koroteev, V. M. Kuznetsov, F. Freyse, J. Sánchez-Barriga, I. R. Amiraslanov *et al.*, *Nature (London)* **576**, 416 (2019).
- [41] C. Koz, S. Rößler, A. A. Tsirlin, S. Wirth, and U. Schwarz, *Phys. Rev. B* **88**, 094509 (2013).
- [42] B. K. Rai, J. Banda, M. Stavinoha, R. Borth, D.-J. Jang, K. A. Benavides, D. A. Sokolov, J. Y. Chan, M. Nicklas, M. Brando, C.-L. Huang, and E. Morosan, *Phys. Rev. B* **98**, 195119 (2018).
- [43] J. Banda, B. K. Rai, H. Rosner, E. Morosan, C. Geibel, and M. Brando, *Phys. Rev. B* **98**, 195120 (2018).
- [44] L. S. Silva, S. G. Mercena, D. J. Garcia, E. M. Bittar, C. B. R. Jesus, P. G. Pagliuso, R. Lora-Serrano, C. T. Meneses, and J. G. S. Duque, *Phys. Rev. B* **95**, 134434 (2017).
- [45] S. L. Bud'ko, V. Zapf, E. Morosan, and P. C. Canfield, *Phys. Rev. B* **72**, 172413 (2005).
- [46] C. Krellner, S. Lausberg, A. Steppke, M. Brando, L. Pedrero, H. Pfau, S. Tencé, H. Rosner, F. Steglich, and C. Geibel, *New J. Phys.* **13**, 103014 (2011).
- [47] J. Diehl, H. Davideit, S. Klimm, U. Tegel, C. Geibel, F. Steglich, and S. Horn, *Phys. B: Condens. Matter* **206–207**, 344 (1995).